Automatic Trajectory Planning of DBS Neurosurgery from Multi-modal MRI Datasets

Silvain Bériault, Fahd Al Subaie, Kelvin Mok, Abbas F. Sadikot, and G. Bruce Pike

McConnell Brain Imaging Centre, Montreal Neurological Institute,
3801 University Street, Montreal, Quebec, H3A 2B4, Canada
silvain.beriault@mail.mcgill.ca

Abstract. We propose an automated method for preoperative trajectory planning of deep brain stimulation image-guided neurosurgery. Our framework integrates multi-modal MRI analysis (T1w, SWI, TOF-MRA) to determine an optimal trajectory to DBS targets (subthalamic nuclei and globus pallidus interna) while avoiding critical brain structures for prevention of hemorrhages, loss of function and other complications. Results show that our method is well suited to aggregate many surgical constraints and allows the analysis of thousands of trajectories in less than 1/10th of the time for manual planning. Finally, a qualitative evaluation of computed trajectories resulted in the identification of potential new constraints, which are not addressed in the current literature, to better mimic the decision-making of the neurosurgeon during DBS planning.

Keywords: Deep brain stimulation, Parkinson's disease, image-guided neurosurgery, automatic planning.

1 Introduction

Over the past decade, Deep Brain Stimulation (DBS) has become a valuable surgical treatment to severe Parkinson's Disease (PD) – a neurodegenerative disease that affects 1% of population over 60 years of age [1] and over one million people in North America [2]. DBS consists of the surgical insertion of stimulation electrodes, in specific nuclei of the basal ganglia circuitry, programmed to reduce PD symptoms. These electrodes are inserted via minimally invasive neurosurgery using precise image guidance from a neuro-navigation platform.

Before the operation, the neurosurgeon undertakes a preoperative planning procedure. The goal is to examine the patient's imaging data to determine: i) precise target locations where to implant the DBS electrodes and ii) safe linear trajectories, from the surface of the head to the targets, that avoid critical structures of the brain to prevent hemorrhages, loss of function and other complications.

Trajectory planning is normally done by manual inspection of a single anatomical MRI dataset using visualization tools offered by commercial neuronavigation platforms. The surgeon empirically searches for a safe trajectory that avoids several critical structures such as: i) the ventricles, ii) deep sulci, iii) large blood vessels, and iv) critical motor and sensory cortex. However, only few trajectories can be thoroughly analyzed in a reasonable amount of time therefore yielding subjective and sub-optimal

G. Fichtinger, A. Martel, and T. Peters (Eds.): MICCAI 2011, Part I, LNCS 6891, pp. 259–266, 2011.

planning. There has been recent interest in the design of automatic planning algorithms to allow the rapid analysis of many more trajectories across multi-modal imaging datasets. With this new paradigm, mimicking the decision-making process of neurosurgeons poses an important challenge.

Proposed methods for automatic planning can be distinguished based on: i) the level of automation, ii) the choice of critical structures and their representation, iii) the trajectory analysis criteria and final scoring, and iv) the overall ease-of-use. Some software tools [3-4] were proposed to simulate the surgical insertion and automatically detect intersected structures, but the entry point selection remains empirical. Many methods encode critical structures once in an atlas [5-7] although recent methods favor direct segmentation in the native patient datasets to better account for inter-subject variability, especially for important structures such as sulci and blood vessels. Very relevant to our work, the method of Brunenberg *et al.* [8] returns many valid trajectories with no further ranking. In the work of Shamir *et al.* [9], trajectories are ranked separately according to either a maximal risk or a sum or risks criteria with no further aggregation. The method of Essert *et al.* [10] automatically ranks trajectories according to several weighted surgical constraints defined by the neurosurgeon using an elaborated extensible markup language (xml) schema. They compare automatic and manual planning according to the final aggregated score, rather than showing how each individual constraint, taken separately, is optimized.

In this work, we present an automatic path planning framework that incorporates several key improvements at every stage of the process: from MRI acquisition to automatic trajectory selection. First, our approach takes advantage of the most recent advances regarding venous and arterial blood vessel imaging with the use of susceptibility weighted imaging (SWI) [11-12] and time-of-flight (TOF) [13] protocols. Second, our trajectory analysis software can handle binary and fuzzy segmentation datasets without the use of a global threshold or of lengthy, iterative, post-processing. Third, our framework meaningfully aggregates several, easy-to-configure, clinical criteria into a single trajectory ranking.

2 Method Overview

Our framework performs multi-modal analysis of patient data to determine the most suitable trajectory to a DBS target according to a set of constraints defined by the surgeon. This section provides detailed information about the multi-modal MRI acquisition protocol, the definition of relevant surgical constraints, and the implementation of the trajectory planning algorithm.

2.1 MRI Acquisition

A multi-modal MRI acquisition protocol is performed on a 3T Siemens TIM Trio with a 32-channel coil. First, a sagittal T1w anatomical scan of the entire head with 1x1x1-mm resolution is obtained using a 3D magnetization-prepared rapid gradient-echo (MP RAGE) sequence (TR=2300ms, TI=900ms, TE=2.98ms, α=9°). Second, a transverse SWI dataset of the brain with 0.5x0.5x1-mm resolution is obtained using a fully flow compensated 3D gradient echo sequence (TR=34ms, TE=20ms, α=12°,

BW=120Hz/px). Third, an MRA dataset is obtained with 1x1x1-mm resolution using a 3D multi-slab TOF (4 slabs, 44 slices/slab, transverse acquisition, TR=22ms, TE=3.85ms, α=18°). These three datasets are acquired in a single session and are aligned by linear registration (rigid body, 6 parameters). Furthermore, the T1w dataset is aligned to the ICBM-152 atlas by non-linear registration [14].

The SWI and TOF sequences provide dense visualization of venous and arterial vasculature (see Fig. 1a-c) without requiring the injection of gadolinium, which adds significant cost to each study and has some associated medical risks. In particular, the SWI sequence (Fig.1a) can image very small veins in comparison to a typical gadolinium protocol (e.g. Fig. 1d). While this dense SWI-TOF protocol allows for a safer trajectory to be planned, the high density makes manual planning a very laborious and challenging task.

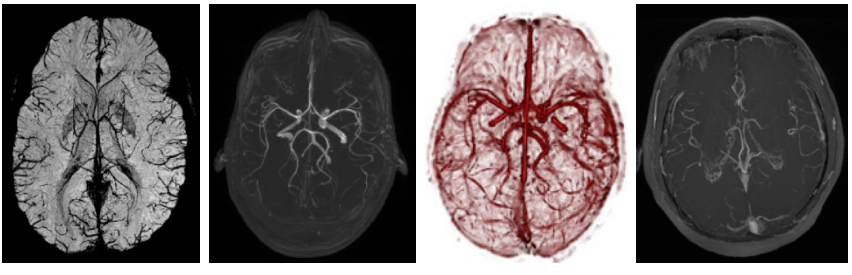

(a) (b) (c) (d)

Fig. 1. SWI-TOF protocol for dense visualization of venous and arterial blood. (a) 30-mm minimum intensity projection (mIP) of an SWI dataset. (b) Maximum intensity projection (MIP) of a TOF dataset. (c) 3D rendering of combined SWI-TOF dataset. (d) 30-mm MIP of a PD patient's clinical scan (T1w with gadolinium).

2.2 Surgical Constraints Definition

Our automatic trajectory planning framework is governed by a set of customizable surgical constraints obtained from multiple interview sessions with a senior neurosurgery resident and an experienced neurosurgeon. These constraints are summarized below. As discussed in Section 4, this list can be further extended and customized as new constraints are found to interplay with the surgeon's decision-making.

1. *Avoid critical cortex area.* To reduce the risk of introducing new neurological deficits, the surgeon typically selects an entry point within the superior frontal lobe, anterior to the primary motor cortex and posterior to the hairline. To mimic this behavior, entry points are limited to a surgeon-chosen region-of-interest (ROI) defined once on the ICBM-152 atlas.
2. *Avoid crossing the midline.* The midline is avoided because it is filled with CSF, it encompasses the thick mid-sagittal sinus vessel and it implicitly eliminates long and risky paths. In our implementation, any entry points on the opposite side of the target are immediately discarded.

3. *Avoid ventricles.* Ventricles are avoided to prevent CSF leaks and to remain in control of the lead. Ventricles are automatically segmented from the T1w dataset using a standard tissue classification method [14].
4. *Avoid blood vessels.* Vessels are avoided to prevent intra-operative complications such as hemorrhages. Veins (SWI dataset) and arteries (TOF dataset) are segmented using a fuzzy vesselness measure [15].
5. *Avoid sulci.* Sulci are avoided because they contain many small vessels that may not be well depicted by current MRI protocols. Sulci are segmented from the T1w dataset using a standard tissue classification method [14].

2.3 Automatic Trajectory Planning

The trajectory planning algorithm consists of analyzing every trajectory linking a set of entry points (on the head surface) to the target. Similarly to work of Essert *et al.* [10], our analysis is conducted in two passes. A first pass quickly eliminates any trajectory that crosses a critical structure at an unsafe distance. With the remaining trajectories, a second pass optimizes the distance to all critical structures simultaneously. Pseudo-code for the second pass is shown at the end of this section.

In other related work [6, 8-10], trajectory optimization is based on a pre-calculated distance map that encodes the minimal distance of a voxel from a critical structure. This method is computationally efficient because the distance map is computed only once and applied to every trajectory. However, this technique only consider the distance to the closest critical structure, therefore giving too much importance to false positive voxels over large clusters representing true critical structures (see Fig. 2 for an example). Furthermore, a distance map can be calculated only on binary segmented datasets. Instead, we represent each trajectory as a cylinder of interest with a N-mm radius (N = 5-mm) i) to account for the dimension of the insertion tool and the precision of patient-to-image registration, and ii) to exclude critical structures already at a safe distance (above 5-mm) without any further processing. With this technique, a distinction can be made between the thick structure of Fig. 2a and the isolated structure of Fig. 2b because, locally, more foreground voxels would intersect the cylinder of interest.

A risk value is given to every voxel inside the cylinder according to the distance from the cylinder's centerline and the voxel value (for fuzzy datasets). For example, the associated risk of a fuzzy vesselness voxel is determined by a combination of: i) its distance from trajectory`s centerline and ii) its vessel-likeliness value. This allows the extraction of many statistical parameters (e.g. $risk_{max}$, $risk_{sum}$, $risk_{mean}$, $risk_{median}$, etc). In this prototype, the maximal risk ($risk_{max}$) and sum of risks ($risk_{sum}$) are extracted and normalized, using a histogram analysis, to a [1 100] range for comparison with other surgical constraints [10]. A final trajectory score is computed by aggregating the $risk_{max}$ and $risk_{sum}$ parameters for all surgical constraints using a weighted cost function (see Algorithm 1). The weights are chosen by the neurosurgeons to represent the relative importance of each constraint. A greater weight is usually given to the $risk_{max}$ criterion because almost hitting a critical structure once is more severe than approaching the same critical structure multiple times at a safer distance [8]. On the other hand, the sum criterion is useful because it distinguishes among cases where a trajectory approaches a critical structure once or multiple times along the path [9].

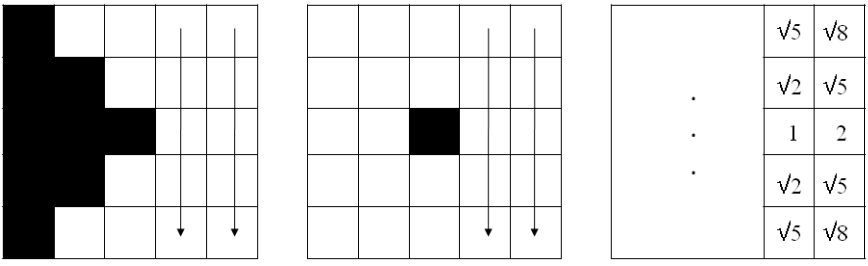

Fig. 2. Distance map calculation fails to distinguish between (a) a true critical structure and (b) an isolated false positive voxel as they both result in the same distance map (c) for the two rightmost columns

Algorithm 1. Trajectory optimization (second pass)

```
Input: ePnts[p];     % list of entry points
Input: tPnt;         % the target point
Input: cs[i];        % list of critical structures
Input: wmax[i];      % weights for each cs (riskMax)
Input: wsum[i];      % weights for each cs (riskSum)
Output: fScores[p]; % final scores for each trajectory
for each p in ePnts
  cylinder = CalcCylinderOfInterest(p, tPnt);
  for each i in cs
    for each j in cylinder
      costs[p][i][j] = CalcCost(cylinder[j], cs[i]);
    riskMax[p][i] = FindMax(costs[p][i][:]);
    riskSum[p][i] = FindSum(costs[p][i][:]);
for each i in cs
  NormalizeToRange(riskMax[:][i], [1 100]);
  NormalizeToRange(riskSum[:][i], [1 100]);
for each p in ePnts
  fScores[p] = 0;
  for each i in cs
    fScores[p]+=riskMax[p][i]*wmax[i];
    fScores[p]+=riskSum[p][i]*wsum[i];
Sort(fScores)
```

3 Experimental Results

Our automatic trajectory planning tool was evaluated by a senior neurosurgery resident and an experienced neurosurgeon. Multi-modal MRI datasets were acquired on two healthy subjects and one patient (M/47 yrs) with severe PD rigidity symptoms. For all subjects, four DBS targets were manually identified by the surgeons – within the two subthalamic nuclei (STN) and the two globus pallidus interna (GPi) – for a total of 12 planning experiments.

First, the senior resident was asked to perform manual trajectory planning of all 12 targets using the commercial Medtronic StealthStation™ software. The same 12 targets were passed to our automatic trajectory planning system. Table 1 shows a quantitative comparison between the risk, on a [1-100] scale, of manual and automatic trajectories with respect to each surgical constraint to remove any bias due to the choice of weights at the final aggregation stage. From Table 1, it is clear that automatically computed trajectory almost always exhibits a smaller risk for all individual criteria of ventricle, sulci and vessel avoidance.

Table 1. Comparison of automatic and manual planning (in parenthesis) for two normal subjects and one severe PD patient. The individual score for each surgical constraint is shown on a [1-100] scale. The automatic trajectory corresponds to the one with the lowest aggregated score and the manual trajectory was found by a senior neurosurgery resident using the Medtronic StealthStation™ platform.

	Target	Ventricles	Sulci		SWI vessels		TOF vessels	
		$risk_{max}$	$risk_{max}$	$risk_{sum}$	$risk_{max}$	$risk_{sum}$	$risk_{max}$	$risk_{sum}$
subj. 0	STN_{left}	1 (15)	2 (4)	2 (34)	1 (1)	7 (25)	3 (1)	10 (15)
	STN_{right}	1 (1)	1 (7)	2 (18)	4 (9)	16 (26)	2 (1)	23 (22)
	GPi_{left}	1 (22)	1 (8)	5 (27)	1 (16)	31 (56)	1 (1)	5 (8)
	GPi_{right}	1 (1)	2 (15)	7 (15)	1 (1)	5 (33)	1 (1)	2 (18)
subj. 1	STN_{left}	1 (31)	7 (22)	7 (57)	8 (9)	7 (27)	1 (1)	12 (49)
	STN_{right}	1 (1)	2 (45)	7 (43)	2 (39)	2 (93)	1 (1)	20 (45)
	GPi_{left}	1 (44)	2 (26)	7 (44)	1 (30)	32 (36)	1 (2)	32 (44)
	GPi_{right}	1 (11)	5 (24)	14 (40)	5 (12)	6 (51)	1 (1)	12 (39)
subj. PD	STN_{left}	1 (1)	5 (46)	13 (42)	4 (16)	37 (41)	2 (1)	5 (28)
	STN_{right}	1 (21)	5 (4)	21 (9)	4 (23)	15 (52)	1 (2)	3 (66)
	GPi_{left}	1 (1)	3 (7)	10 (24)	1 (1)	24 (54)	1 (2)	5 (35)
	GPi_{right}	12 (11)	1 (33)	3 (29)	4 (30)	5 (79)	1 (11)	12 (5)

Second, both surgeons were asked to qualitatively evaluate the 12 automatic trajectories selected by our software. This was done using 3D visualization software we developed and also by supplying the trajectories to the Medtronic StealthStation software because surgeons were most familiar with this platform. The surgeons found our automatic method more effective than manual planning for simultaneous avoidance of all critical structures. For examples: i) the manual trajectories to subject 0's STN_{left} and GPi_{left} travel near the ventral horn of the lateral ventricles; ii) because of subject 1's complex gyri pattern, manual sulci avoidance was sometime at a distance <1.5mm (instead of >2.5 mm with automatic planning), iii) the PD case exhibited larger ventricles and some brain atrophy, making the manual search more challenging.

Interestingly, the surgeons were able to identify new problems that are not handled by the current set of implemented constraints. For few suggested trajectories, they argued they would prefer a trajectory that is either more medial or that can avoid other basal ganglia nuclei (caudate, putamen). Only one suggested trajectory was found unsuitable because it was running parallel to a sulcus, at a safe distance, but in a way where a longer stretch of frontal lobe's cortex (grey matter) was traversed which could increase the risk of causing new neurological deficits.

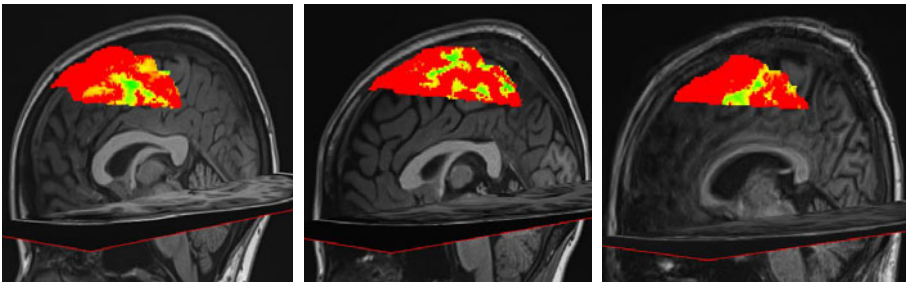

Subject 0 Subject 1 PD patient

Fig. 3. Examples of color-coded trajectory map generated by our software. Color scale: green=recommended, yellow=acceptable, red=rejected.

4 Discussion and Conclusions

From the quantitative analysis of Table 1, it is clear that automatic planning outperforms manual planning with the task of aggregating several, well-defined, surgical constraints. Furthermore, automatic planning allows for thousands of trajectories (~12000) to be thoroughly analyzed in less than 4 minutes whereas manual planning approximately requires over 40 minutes per target.

Our experimental results showed that this quantitative analysis alone does not assess whether the implemented constraints mimic the complete decision-making process of neurosurgeons. Indeed, a qualitative analysis revealed the presence of previously undescribed surgical constraints. Fortunately, when an issue was raised an alternate entry point could easily be selected using the intuitive color-coded map outputted by our framework (see Fig. 3). In addition, we were able to eliminate most of these exceptional situations by adapting some of the user parameters. For example, we can force our software to find a more medial entry point simply by reducing the initial search to a more medial ROI.

In conclusion, manual path planning, especially with dense multi-modal datasets, is a complex and lengthy process that yields subjective and potentially sub-optimal solutions. This work provides neurosurgeons with an intuitive decision support system for automatic planning of DBS neurosurgeries that aggregates multiple surgical requirements into a single weighted ranking of available trajectories. Future work will concentrate on optimizing the weights attributed to each surgical constraint and on integrating additional constraints that were found to interplay with the decision-making process of surgeons to avoid long stretches of grey matter cortex and other basal ganglia nuclei (caudate and putamen).

Acknowledgement. This research was funded by the Natural Sciences and Engineering Research Council of Canada and the Centres of Excellence for Commercialization and Research.

References

1. de Lau, L.M.L., Breteler, M.M.B.: Epidemiology of Parkinson's disease. The Lancet Neurology 5, 525–535 (2006)
2. Chou, K.L.: Indication for Subthalamic Nucleus Deep Brain Stimulation Surgery. In: Baltuch, G.H., Stern, M.B. (eds.) Deep Brain Stimulation for Parkinson's Disease, pp. 41–54. informa healthcare, New York (2007)
3. Lee, J.D., Huang, C.H., Lee, S.T.: Improving stereotactic surgery using 3-D reconstruction. IEEE Eng. Med. Biol. Mag. 21, 109–116 (2002)
4. Nowinski, W.L., Yang, G.L., Yeo, T.T.: Computer-aided stereotactic functional neurosurgery enhanced by the use of the multiple brain atlas database. IEEE Trans. Med. Imaging 19, 62–69 (2000)
5. Fujii, T., Emoto, H., Sugou, N., Mito, T., Shibata, I.: Neuropath planner-automatic path searching for neurosurgery. International Congress Series 1256, 587–596 (2003)
6. Tirelli, P., De Momi, E., Borghese, N.A., Ferrigno, G.: An intelligent atlas-based planning system for keyhole neurosurgery. International Journal of Computer Assisted Radiology and Surgery 4, S85–S91 (2009)
7. Vaillant, M., Davatzikos, C., Taylor, R., Bryan, R.: A path-planning algorithm for image-guided neurosurgery. In: Troccaz, J., Mösges, R., Grimson, W.E.L. (eds.) CVRMed-MRCAS 1997, CVRMed 1997, and MRCAS 1997. LNCS, vol. 1205, pp. 467–476. Springer, Heidelberg (1997)
8. Brunenberg, E.J.L., Vilanova, A., Visser-Vandewalle, V., Temel, Y., Ackermans, L., Platel, B., ter Haar Romeny, B.M.: Automatic Trajectory Planning for Deep Brain Stimulation: A Feasibility Study. In: Ayache, N., Ourselin, S., Maeder, A. (eds.) MICCAI 2007, Part I. LNCS, vol. 4791, pp. 584–592. Springer, Heidelberg (2007)
9. Shamir, R.R., Tamir, I., Dabool, E., Joskowicz, L., Shoshan, Y.: A Method for Planning Safe Trajectories in Image-Guided Keyhole Neurosurgery. In: Jiang, T., Navab, N., Pluim, J.P.W., Viergever, M.A. (eds.) MICCAI 2010. LNCS, vol. 6363, pp. 457–464. Springer, Heidelberg (2010)
10. Essert, C., Haegelen, C., Jannin, P.: Automatic Computation of Electrodes Trajectory for Deep Brain Stimulation. In: Liao, H., Edwards, P.J., Pan, X., Fan, Y., Yang, G.-Z. (eds.) MIAR 2010. LNCS, vol. 6326, pp. 149–158. Springer, Heidelberg (2010)
11. Haacke, E.M., Xu, Y., Cheng, Y.C., Reichenbach, J.R.: Susceptibility weighted imaging (SWI). Magn. Reson. Med. 52, 612–618 (2004)
12. Haacke, E.M., Mittal, S., Wu, Z., Neelavalli, J., Cheng, Y.C.: Susceptibility-weighted imaging: technical aspects and clinical applications, part 1. AJNR Am J. Neuroradiol. 30, 19–30 (2009)
13. Graves, M.J.: Magnetic resonance angiography. Br J. Radiol. 70, 6–28 (1997)
14. Collins, D.L., Zijdenbos, A.P., Baaré, W.F.C., Evans, A.C.: ANIMAL+INSECT: Improved Cortical Structure Segmentation. In: Kuba, A., Sámal, M., Todd-Pokropek, A. (eds.) IPMI 1999. LNCS, vol. 1613, pp. 210–223. Springer, Heidelberg (1999)
15. Frangi, A.F., Niessen, W.J., Vincken, K.L., Viergever, M.A.: Multiscale vessel enhancement filtering. In: Wells, W.M., Colchester, A.C.F., Delp, S.L. (eds.) MICCAI 1998. LNCS, vol. 1496, pp. 130–137. Springer, Heidelberg (1998)